RSC Advances

PAPER

View Article Online
View Journal | View Issue

Cite this: *RSC Adv.*, 2017, **7**, 29035

Mechanistic study on ligand-controlled copper-catalyzed regiodivergent silacarboxylation of allenes with carbon dioxide and silylborane†

Shu-Min Han,[a] Xingdong Wang,[b] Shenhua Miao,*[a] Zhang-Yu Yu[ab] and Tao Liu *[ab]

Recently, Tsuji and co-workers reported a ligand controlled regiodivergent silacarboxylation of allenes with CO_2 and a silylborane in the presence of a copper catalyst. Product P_1 was generated in the *rac*-Me-DuPhos (L_A) assisted system while product P_2 was obtained in the PCy_3 (L_B) assisted system. To account for the observed regioselectivity, density functional theory (DFT) calculations have been carried out in the present study. We calculated the detailed mechanisms and analyzed electronic and steric factors in the selectivity-determining states **TS3A**, **TS9A**, **TS2B**, and **TS5B** to gain insight into the origin of the observed regioselectivity. For the L_A-assisted system, the regioselectivity is predicted to be determined by the great steric effects of **TS9A**. The more stable geometry of **TS3A** causes P_1 to be the major product. For the L_B-assisted system, electronic effects can account for the regioselectivity. The stronger attractive interaction in **TS5B** compared with that in **TS2B** leads to the generation of P_2.

Received 31st March 2017
Accepted 28th May 2017

DOI: 10.1039/c7ra03723f

rsc.li/rsc-advances

1. Introduction

As useful building blocks in organic synthesis, organosilanes can undergo a good deal of silicon-assisted transformations.[1] In particular, silylcupration of C–C multiple bonds (especially the allene derivatives) has become one of the most reliable and powerful procedures that forms both vinyl- and allyl-silanes.[2] However, how to control the selectivity has become the serious problem since the addition reactions across unsaturated substrates often result in many regio- and stereo-isomers.[2g,3] The first-row transition metals have often been used as catalysts to solve the problem,[4] not only due to their considerably low price, but the differing electronic structures of 3d transition metals provide promise for developing significant molecular structures and uncovering new organometallic reactivities at a fundamental level.[5] In addition, as a greenhouse gas providing serious harm to the environment, carbon dioxide (CO_2) capture, utilization, and conversion have become hot topics in research.[6]

Recently, Tsuji and co-workers reported a ligand controlled regiodivergent silacarboxylation of allenes with CO_2 and a silylborane in the presence of a copper catalyst (Scheme 1).[7] As shown in Scheme 1, the ratio of two different products $\mathbf{P_1}$ and $\mathbf{P_2}$ can be highly controlled by the proper choice of ligand. The major product is $\mathbf{P_1}$ in reaction condition A (when Cu(OAc) is used as the catalyst precursor, hexan as the solvent, and the *rac*-Me-DuPhos ($\mathbf{L_A}$) as the ligand). In contrast, the major product is changed to $\mathbf{P_2}$ when a mixture of CuCl/NaOAc was used as the catalyst precursor, THF as the solvent, and PCy_3 ($\mathbf{L_B}$) as the ligand (reaction condition B, Scheme 1).

To account for the observed regioselectivity of this reaction, a plausible mechanism has been proposed by Tsuji *et al.*[7] As shown in Scheme 2, a Cu catalyst precursor first reacts with one reactant **R1** to form a silylcopper complex **1**. Next, another reactant **R2** coordinates to the Cu center of **1** *via* the terminal double bond and generates two isomers **2** and **5** according to the orientation of the unsymmetrical allene **R2**, which is followed by the subsequent alkene insertion to form the allylcopper complex **3** and vinylcopper complex **6**, respectively. With CO_2 inserting at the γ-position of **3**, copper carboxylate complex **4** is afforded. Finally, through the σ-bond metathesis between **4** and **R1**, boron carboxylate $\mathbf{P_{0-1}}$ is produced, accompanied with the **1** regenerating. Through the conversion with H_3O^+ and Me_3SiCHN_2 further, $\mathbf{P_{0-1}}$ could afford the final product $\mathbf{P_1}$. In contrast, the insertion of CO_2 into **6** generates intermediate **7**, followed by the σ-bond metathesis with **R1** to provide boron carboxylate $\mathbf{P_{0-2}}$ and regenerate **1**. Finally, final product $\mathbf{P_2}$ could be obtained through the further conversion of $\mathbf{P_{0-2}}$ with H_3O^+ and Me_3SiCHN_2.

Although a plausible mechanistic pathway has been proposed by Tsuji group, some key issues still need to be further discussed. (1) What is the detailed reaction mechanism? (2) How is the origin of this high ligand-controlled regioselectivity? Here we would like to report our detailed density functional theory (DFT) calculations on the reaction mechanisms in order to gain insight into the interesting experimental observations

[a]*School of Chemistry and Chemical Engineering, Qufu Normal University, Qufu 273165, Shandong, China. E-mail: liutao_2005@126.com*

[b]*Department of Chemistry and Chemical Engineering, Jining University, Qufu 273155, Shandong, China*

† Electronic supplementary information (ESI) available. See DOI: 10.1039/c7ra03723f

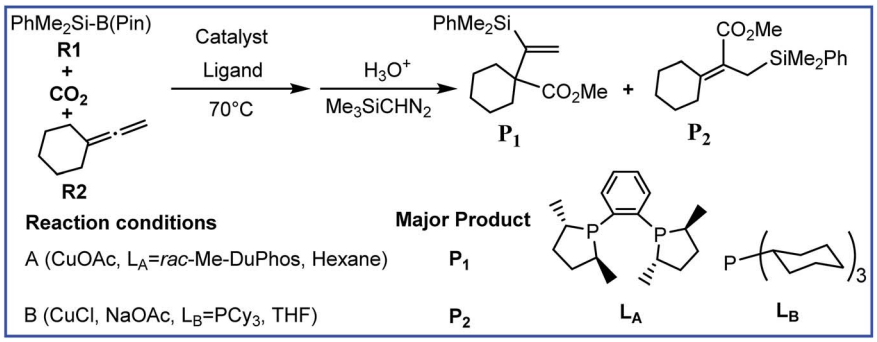

Scheme 1 Cu-catalyzed silacarboxylation of allenes with CO_2 and silylborane reported by Tsuji group.

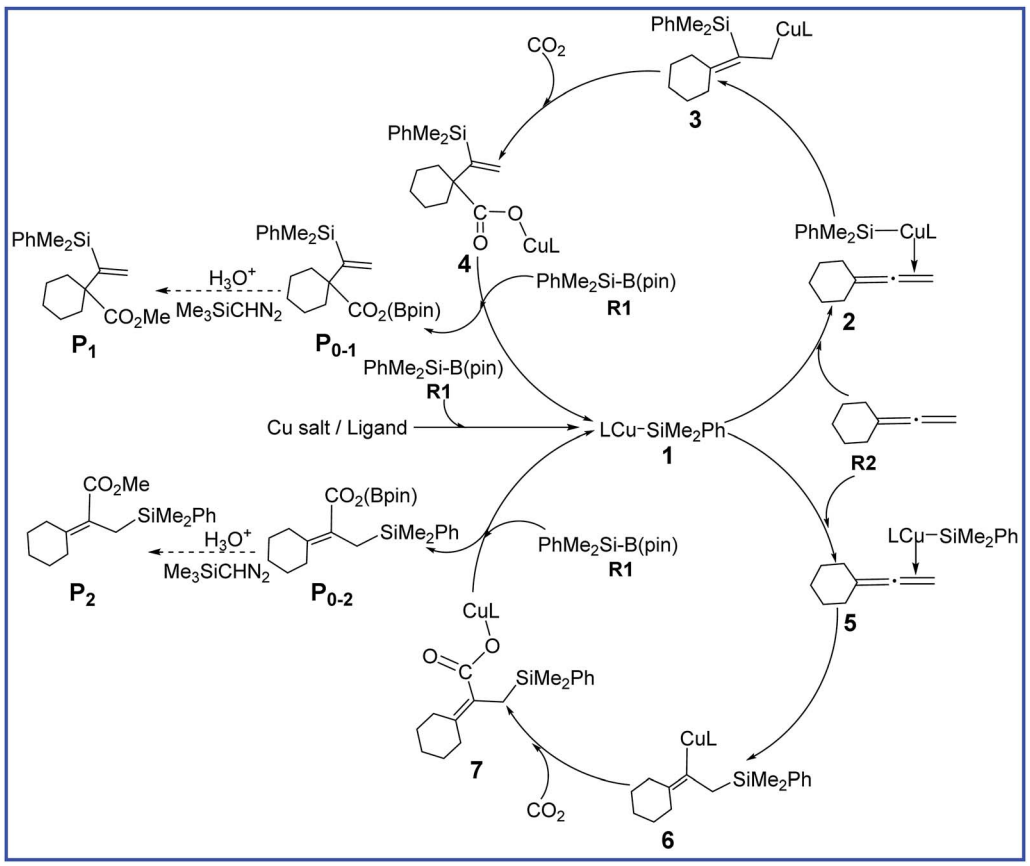

Scheme 2 Mechanisms of Cu-catalyzed silacarboxylation of allenes with CO_2 and silylborane proposed by Tsuji group.

and distinct selectivity. We expect this work would help understand the detailed mechanisms and design new related reactions.

2. Computational details

In our calculations, the geometries of all intermediates and transition states were optimized at the B3LYP[8] level of DFT in gas phase. A mixed basis set of 6-311+G(d) for Cu and 6-31G(d,p) for other atoms (BSI) was used, which has been proved to be appropriate for the copper-catalyzed reactions.[9] Frequency analysis were carried out to ensure all stationary points as minima (zero imaginary frequencies) or transition states (one imaginary frequency) at the B3LYP/BSI level. When necessary, intrinsic reaction coordinates (IRC)[10] calculations were applied for transition state to confirm it actually connecting the corresponding two minima. To consider solvent effects, we performed single-point energy calculations for all the gas-phase optimized structures with SMD[11] solvent model at the M06 (ref. 12)/BSII (6-311+G(d) for Cu and 6-311++G(d,p) for other atoms) level. Natural bond orbital (NBO)[13] charges were calculated for selected structures at the M06/BSII level. Free energies (kcal mol^{-1}) obtained at the M06/BSII//B3LYP/BSI level were used in

the following discussion. All the calculations were carried out with the GAUSSIAN 09 packages.[14]

3. Results and discussion

In this work, we first investigate the **Cu/L$_A$**-catalyzed mechanisms leading to **P$_{0-1}$** and **P$_{0-2}$**, respectively (reaction A). Then we study the reaction mechanisms catalyzed by **Cu/L$_B$** (reaction B) to probe the regioselectivity observed experimentally.

3.1 Cu/L$_A$-catalyzed reaction mechanisms

The free energy diagrams for the reaction to lead to product **P$_{0-1}$** catalyzed by **Cu/L$_A$** are calculated and shown in Fig. 1. Firstly, the precatalyst CuOAc (**1A**) coordinates with the ligand **L$_A$** to form the active catalyst **2A** by releasing the free energy of 57.0 kcal mol^{-1}. Subsequently, the transmetalation of **2A** with **R1** occurs to generate a three-coordinate Cu(I) intermediate **3A** and dissociate the complex B(pin)–OAc, through a concerted four-centered transition state **TS1A** related to σ-bond metathesis. This step is thermodynamically and kinetically feasible, with free energy decreasing of 6.8 kcal mol^{-1} as well as an attainable activation free energy (8.6 kcal mol^{-1}). The terminal double bond of reactant **R2** then coordinates to the Cu center of silylcopper intermediate **3A** along with the dissociation of one arm of **L$_A$**[15–17] *via* the transition state **TS2A** and generates intermediate **4A** with a barrier of 8.6 kcal mol^{-1}. The subsequent alkene insertion step requires a low activation energy barrier of 7.5 kcal mol^{-1} *via* transition state **TS3A** to form the allylcopper intermediate **5A**. The energy barrier is 14.4 kcal mol^{-1} for the migratory insertion step (**3A** → **TS3A**). In the next step, CO_2 inserts at the γ-position of **5A** to a provide copper carboxylate complex **7A** *via* a six-membered-ring transition state **TS4A** with the activation energy barrier of 12.2 kcal mol^{-1}. The stepwise pathway for the CO_2 insertion step (CO_2 first inserting into the C–Cu bond of **5A** to give carboxylate intermediate **6A**, which then undergoing a [1,3]-sigmatropic rearrangement to afford **7A**) was also considered (see the red line in Fig. 1), but the calculated results indicates that such a proposal is inaccessible due to the forbidden high barrier (87.8 kcal mol^{-1}). Finally, **7A** combines with **R1** to form intermediate **8A**, which then produces boron carboxylate **P$_{0-1}$** and regenerates **3A** *via* a σ-bond metathesis transition state **TS7A** with an attainable free energy barrier 13.3 kcal mol^{-1}. Through the conversion with H_3O^+ and Me_3SiCHN_2 further, **P$_{0-1}$** could afford the final product **P$_1$**. As shown in Fig. 1,

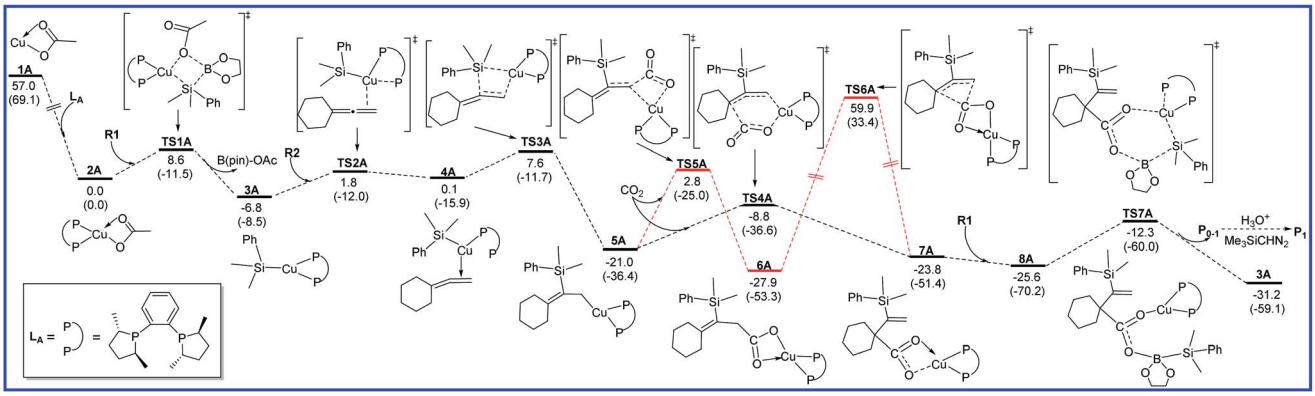

Fig. 1 Free energy diagrams to lead to P$_{0-1}$ catalyzed by Cu/L$_A$. The relative free energies and relative enthalpic energies (in parentheses) are given in kcal mol^{-1}.

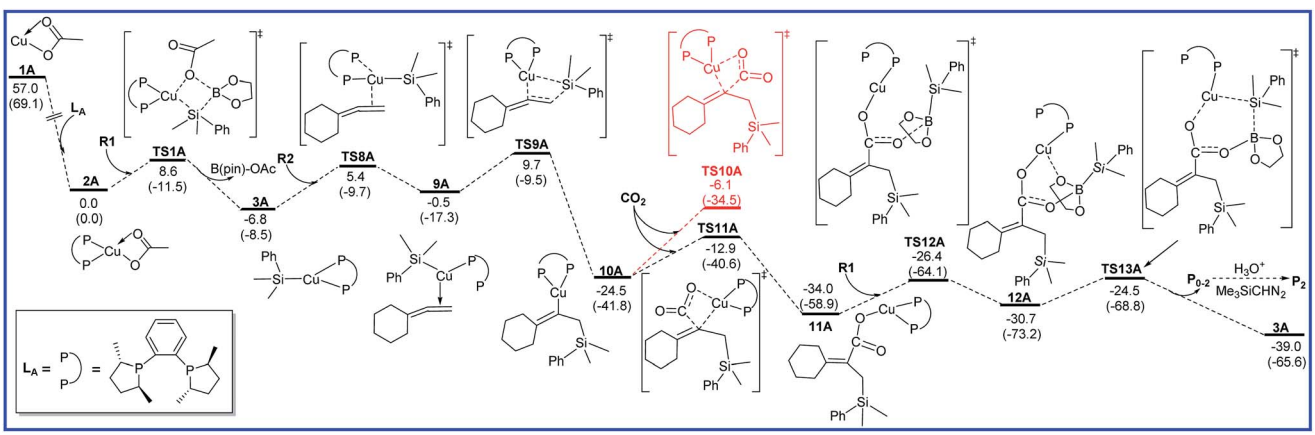

Fig. 2 Free energy diagrams to lead to P$_{0-2}$ catalyzed by Cu/L$_A$. The relative free energies and relative enthalpic energies (in parentheses) are given in kcal mol^{-1}.

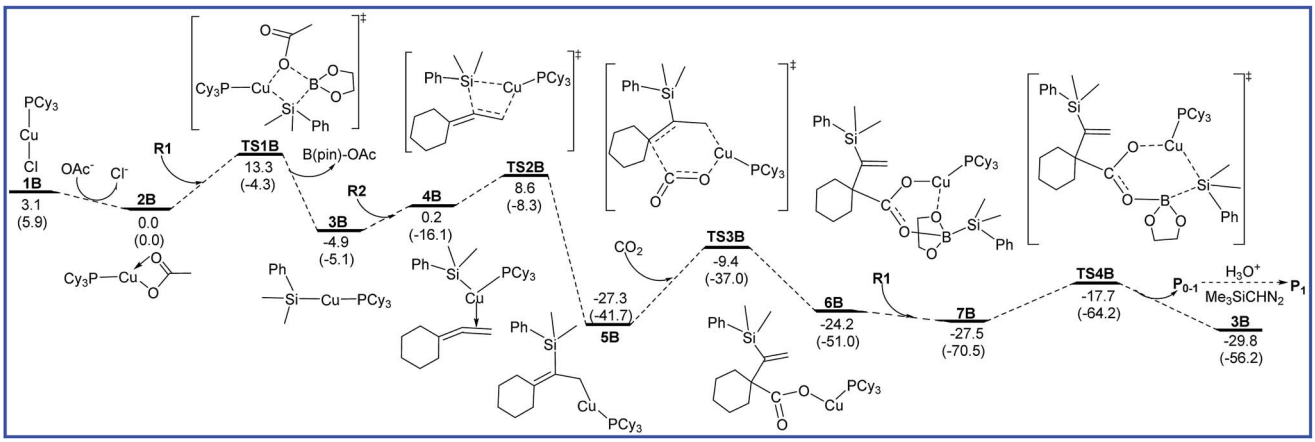

Fig. 3 Free energy diagrams to lead to P_{0-1} catalyzed by Cu/L_B. The relative free energies and relative enthalpic energies (in parentheses) are given in kcal mol^{-1}.

the rate-determining step in reaction A to produce $\mathbf{P_{0-1}}$ is the alkene migratory insertion step (**3A** → **TS3A**) and the overall activation barrier is 14.4 kcal mol^{-1}.

As shown in Fig. 2, **R2** can also coordinate with **3A** *via* another conformation to produce intermediate **9A** with a barrier of 12.2 kcal mol^{-1} (**TS8A**). An intramolecular migratory insertion then occurs to form the vinylcopper intermediate **10A** through the transition state **TS9A**, which requires the activation energy barrier of 10.2 kcal mol^{-1}. In the following step, CO_2 inserts into the C–Cu bond of **10A** to afford a copper carboxylate intermediate **11A** through a four-membered-ring transition state **TS11A** with a free energy barrier of 11.6 kcal mol^{-1}. Herein, another CO_2 insertion transition state **TS10A** was excluded due to the higher free energy compared with **TS11A** (−6.1 *vs.* −12.9 kcal mol^{-1}). Then, **11A** binds up with **R1** to form intermediate **12A**, followed by the σ-bond metathesis (**TS13A**) to afford boron carboxylate $\mathbf{P_{0-2}}$ and regenerate **3A** with an attainable free energy barrier 9.5 kcal mol^{-1}. Finally, final product $\mathbf{P_2}$ could be obtained through the further conversion of $\mathbf{P_{0-2}}$ with H_3O^+ and Me_3SiCHN_2. It can be found from Fig. 2 that the alkene migratory insertion process (**3A** → **TS9A**) is also the rate-determining step with the overall activation barrier of 16.5 kcal mol^{-1} in reaction A leading to product $\mathbf{P_{0-2}}$.

Taking the full process shown in Fig. 1 and 2 into account, the alkene migratory insertion step is the regioselectivity-determining step, and the competition between **TS3A** and **TS9A** determines the regioselectivity ($\mathbf{P_{0-1}}$ or $\mathbf{P_{0-2}}$). The calculated free energy difference (2.1 kcal mol^{-1}) between **TS3A** and **TS9A** is reasonable agreement with the experimental major product $\mathbf{P_1}$.

3.2 Cu/L_B-catalyzed reaction mechanism

The free energy diagrams for the reaction leading to $\mathbf{P_{0-1}}$ catalyzed by $\mathbf{Cu/L_B}$ are shown in Fig. 3. At the entrance of the reaction, precatalyst PCy_3CuCl (**1B**) transforms into the active catalyst PCy_3CuOAc (**2B**) *via* the ligand substitution with the additive NaOAc. This process is exoergic by 3.1 kcal mol^{-1}. **2B** sequentially undergoes σ-bond metathesis with **R1** to give the intermediate **3B** with a barrier of 13.3 kcal mol^{-1}. The transmetalation pathway of **1B** with **R1** was also considered, but the calculated high barrier rules out the possibility (see Fig. S1 in

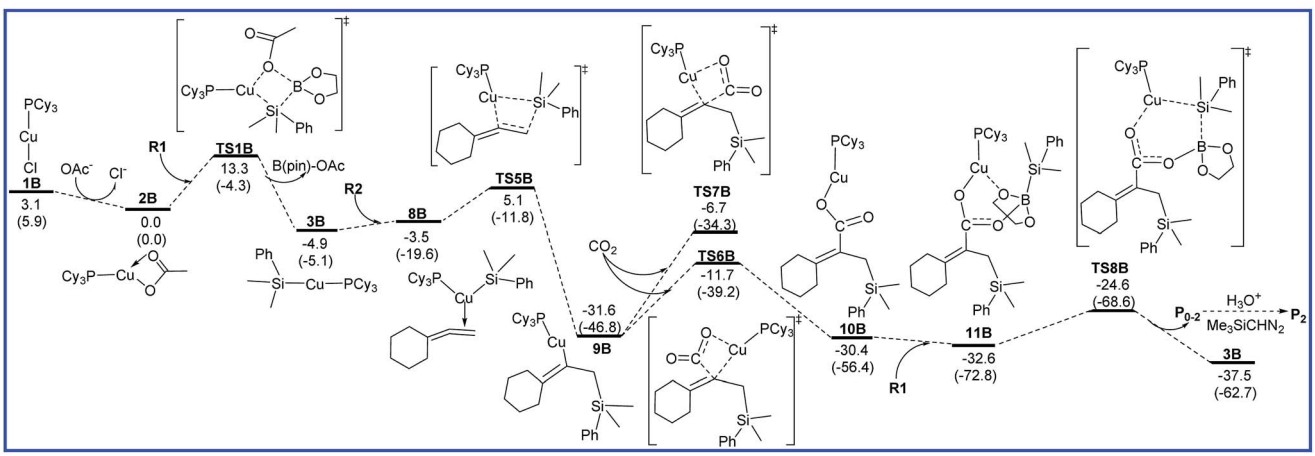

Fig. 4 Free energy diagrams to lead to P_{0-2} catalyzed by Cu/L_B. The relative free energies and relative enthalpic energies (in parentheses) are given in kcal mol^{-1}.

Table 1 Regioselectivity-determining and rate-determining steps in reactions A and B, along with related activation energies (kcal mol^{-1})

Reactions	Major product	Regioselectivity-determining step[a] ($\Delta G_1^{\ddagger}$)			Rate-determining step[b] ($\Delta G_2^{\ddagger}$)		
Reaction A (**Cu/L$_A$**)	**P$_1$**	Alkene insertion	**3A** → **TS3A**	(14.4)	Alkene insertion	**3A** → **TS3A**	(14.4)
			3A → **TS9A**	(16.5)		**3A** → **TS9A**	(16.5)
Reaction B (**Cu/L$_B$**)	**P$_2$**	Alkene insertion	**3B** → **TS2B**	(13.5)	CO_2 insertion	**5B** → **TS3B**	(17.9)
			3B → **TS5B**	(10.0)		**9B** → **TS6B**	(19.9)

[a] $\Delta G_1^{\ddagger}$, Gibbs free activation energy of rate-determining step. [b] $\Delta G_2^{\ddagger}$, Gibbs free activation energy of rate-determining step.

ESI†). Then, **R2** inserts into the Cu–Si bond *via* transition state **TS2B** to form a allylcopper intermediate **5B**. The energy barrier of insertion process is 13.5 kcal mol^{-1}. The following CO_2 insertion step requires the energy barrier of 17.9 kcal mol^{-1} to generate a copper carboxylate intermediate **6B** *via* a six-membered-ring transition state **TS3B**. Finally, σ-bond metathesis of **6B** with **R1** occurs to afford boron carboxylate **P$_{0-1}$** and regenerate **3B** with a free energy barrier 9.8 kcal mol^{-1}. As shown in Fig. 3, the rate-determining step for the reaction leading to **P$_{0-1}$** catalyzed by **Cu/L$_B$** is CO_2 insertion (**5B** → **TS3B**), and the overall energy barrier is 17.9 kcal mol^{-1}.

The free energy diagrams for the reaction leading to **P$_{0-2}$** catalyzed by **Cu/L$_B$** are shown in Fig. 4. From intermediate **3B**, the regioselectivity occurs. **R2** inserts into the Cu–Si bond of **3B** towards another orientation *via* the transition state **TS5B** to form the vinylcopper intermediate **9B** with an energy barrier of 10.0 kcal mol^{-1}. Then, CO_2 inserts into the C–Cu bond of **9B** through a four-membered-ring transition state **TS6B** to form a copper carboxylate intermediate **10B** with a free energy barrier of 19.9 kcal mol^{-1}. Another transition state **TS7B** for the CO_2 insertion step was also calculated, but the higher relative free energy (6.1 kcal mol^{-1}) indicates that this pathway is infeasible. Finally, **10B** binds up with **R1** to generate intermediate **11B**, which is followed by the σ-bond metathesis (**TS8B**) to afford boron carboxylate **P$_{0-2}$** and regenerate **3B** with an attainable free energy barrier 8.0 kcal mol^{-1}. As shown in Fig. 4, for the reaction leading to **P$_{0-2}$** catalyzed by **Cu/L$_B$**, the CO_2 insertion process is found to be the rate-determining step with the overall activation barrier of 19.9 kcal mol^{-1} (**9B** → **TS6B**).

As shown in Fig. 3 and 4, the regioselectivity-determining steps to lead to **P$_{0-1}$** and **P$_{0-2}$** catalyzed by **Cu/L$_B$** are **3B** → **TS2B** (13.5 kcal mol^{-1}) and **3B** → **TS5B** (10.0 kcal mol^{-1}), respectively. The relative free energy difference (3.5 kcal mol^{-1}) between **TS2B** and **TS5B** is reasonable agreement with the experimental major product **P$_2$**.

Other possible pathways were also considered. For example, in the transmetalation process of **1B** and **R1**, the pathway that PCy_3Cu moiety attacking toward B(pin) moiety, accompanied with the **R1** moiety attacking toward Cl moiety was also considered, but the calculated results indicated that such a proposal is inaccessible (see Fig. S2 in ESI†). The inaccessible pathways that CO_2 insertion prior to the alkene insertion step were also calculated (see Fig. S3 in ESI†). The impact of additive NaOAc on the regioselectivity was also calculated and ruled out (see Fig. S4 in ESI†).

In order to give a clear picture, the mechanistic scenarios for reactions A and B are summarized in Table 1. For reactions A and B, the regioselectivity-determining and rate-determining steps together with activation energy barriers are presented. It can be seen from the table that the regioselectivity-determining step is the reaction of **3A** (**3B**) and **R2** process, which is the divergence of **P$_{0-1}$** and **P$_{0-2}$**. In addition, we can see all the reverse reactions of **3A** (**3B**) and **R2** are unachievable kinetically with too high activation energies from the preceding energy diagrams. Consequently, it is predictive that reactions of **3A** (**3B**) and **R2** are irreversible and thus this divergent step determines the major product (**P$_1$** or **P$_2$**). In other words, the major product is determined by the relative stability of the two divergent transition states from reaction of **3A** (**3B**) and **R2**.

For **Cu/L$_A$**-catalyzed reaction A, generation of **P$_1$** is calculated to be kinetically more favored than that of **P$_2$**. The activation energy barrier difference between the two reactions is 2.1 kcal mol^{-1} (**TS3A** *vs.* **TS9A**). The rate-determining steps are same to the regioselectivity-determining steps which predicted to be the alkene insertion for the two reactions. For **Cu/L$_B$** reaction B, **P$_2$** becomes the major product, and the activation energy difference between the two reactions of **3B** + **R2** is enlarged to 3.5 kcal

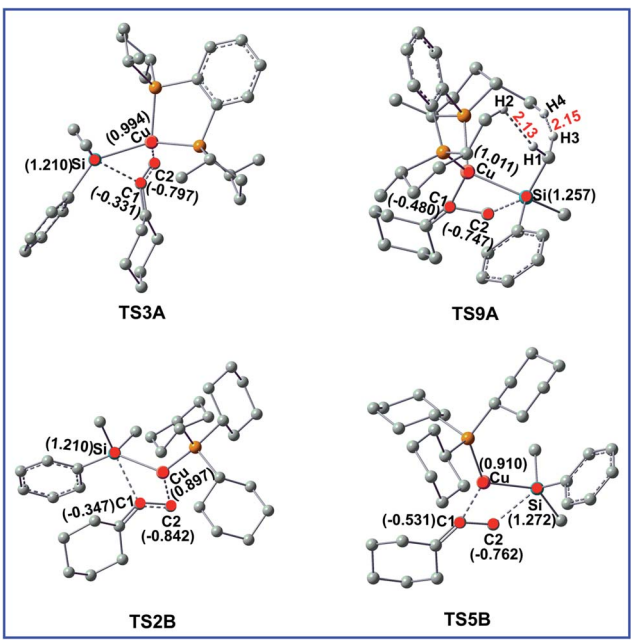

Fig. 5 Optimized structures for the transition states TS3A, TS9A, TS2B, and TS5B. Some important bond distances are given in Å. The hydrogen atoms not participating in the reaction have been omitted for clarity. The values in parentheses are the related NBO charges (in *e*).

mol^{-1}. The rate-determining step is CO_2 insertion process for the two reactions.

3.3 Origin of the regioselectivity

To gain insight into the origin of the observed regioselectivity, we checked both steric and electronic effects in the selectivity-determining transition states **TS3A**, **TS9A**, **TS2B**, and **TS5B**. The important bond distances and NBO charges for the four transitions states are shown in the Fig. 5.

For **Cu/L$_A$**-catalyzed reaction A, the steric effects are the major factors to account for the regioselectivity. As shown in Fig. 5, the H1⋯H2 and H3⋯H4 distances in **TS9A** are 2.13 and 2.15 Å, respectively, which are less than the sums of the van der Waals radii of hydrogen (1.20 Å). Thus, the great steric effects destabilize **TS9A** and rule out the possibility to lead to **P$_2$** product in this reaction. In contrast, there are no obvious electronic effects difference in **Cu/L$_A$**-catalyzed reaction (**TS3A** and **TS9A**).

For **Cu/L$_B$**-catalyzed reaction B, there are no obvious steric bias both in **TS2B** and **TS5B**. Compared the corresponding NBO charges in Fig. 5, it can be found that the Cu atom become more negatively charged when the attached ligand **L$_A$** is replaced by **L$_B$**. As shown in Fig. 5, more negative C2 atom combines with the less positive Cu atom in **TS2B**, while combines with the more positive atom Si in **TS5B**. Obviously, the stronger attractive interaction caused by electronic factors in **TS5B** leads to the major product **P$_2$**.

4. Conclusions

We have presented a detailed and plausible mechanism for the copper-catalyzed ligand controlled regiodivergent silacarboxylation of allenes with CO_2 and silylborane by using DFT calculations. Two reactions are included in this study, reactions A (CuOAc as the catalyst and product **P$_1$** is favored with the bidentate **L$_A$** ligand), and B (CuCl/NaOAc as the catalyst and product **P$_2$** is favored with the monodentate **L$_B$** ligand). The rate-determining steps for the reactions to form products **P$_1$** and **P$_2$** catalyzed by **Cu/L$_A$** both are the alkene insertion step, while rate-determining steps for the reactions catalyzed by **Cu/L$_B$** both are the CO_2 insertion step.

The origin of the experimentally observed selectivity on different products has been analyzed based on the above mechanistic details. It is found that regioselectivity depends on the relative feasibility of alkene migratory insertion step. For **Cu/L$_A$**-catalyzed system, the generation of product **P$_1$** is preferred mainly due to the great steric effects of **TS9A** that rule out the possibility to lead to **P$_2$**. For **Cu/L$_B$**-catalyzed system, electronic effects become the major factors to produce the major product **P$_2$**. The in-depth understanding for the divergent reaction mechanisms and distinct regiochemistry could be beneficial in designing new related reactions.

Acknowledgements

This work was jointly supported by Natural Science Foundation of Shandong Province (No. ZR2014BM038), and Talent Team Culturing Plan for Leading Disciplines of University in Shandong Province.

References

1 (*a*) T. Liu and S. W. Bi, *Organometallics*, 2016, **35**, 1114; (*b*) R. Alam, T. Vollgraff, L. Eriksson and K. J. Szabó, *J. Am. Chem. Soc.*, 2015, **137**, 11262; (*c*) M. Yus, J. C. González-Gómez and F. Foubelo, *Chem. Rev.*, 2013, **113**, 5595; (*d*) I. Beletskaya and C. Moberg, *Chem. Rev.*, 2006, **106**, 2320.

2 (*a*) W. M. Yuan, S. Liu and S. M. Ma, *Angew. Chem., Int. Ed.*, 2016, **55**, 3140; (*b*) J. Rae, Y. C. Hu and D. J. Procter, *Chem.–Eur. J.*, 2014, **20**, 13143; (*c*) J. A. Calderone and W. L. Santos, *Angew. Chem., Int. Ed.*, 2014, **53**, 4154; (*d*) Y. H. Xu, L. H. Wu, J. Wang and T. P. Loh, *Chem. Commun.*, 2014, **50**, 7195; (*e*) A. Barbero and F. J. Pulido, *Acc. Chem. Res.*, 2004, **37**, 817; (*f*) M. Y. Wu, F. Y. Yang and C. H. Cheng, *J. Org. Chem.*, 1999, **64**, 2471; (*g*) E. Langkopf and D. Schinzer, *Chem. Rev.*, 1995, **95**, 1375.

3 (*a*) M. Uehling, R. Rucker and G. Lalic, *J. Am. Chem. Soc.*, 2014, **136**, 8799; (*b*) S. C. Yu and S. M. Ma, *Angew. Chem., Int. Ed.*, 2012, **51**, 3074.

4 (*a*) C. C. Xia, K. Wang, J. Xu, C. Shen, D. Sun, H. S. Li, G. D. Wang and P. F. Zhang, *Org. Biomol. Chem.*, 2017, **15**, 531; (*b*) T. Itoh, Y. Shimizu and M. Kanai, *J. Am. Chem. Soc.*, 2016, **138**, 7528; (*c*) M. Pirnot, Y. Wang and S. Buchwald, *Angew. Chem., Int. Ed.*, 2016, **55**, 48; (*d*) R. Bullock and M. Helm, *Acc. Chem. Res.*, 2015, **48**, 2017; (*e*) K. Semba, T. Fujihara, J. Terao and Y. Tsuji, *Angew. Chem., Int. Ed.*, 2013, **52**, 12400.

5 (*a*) M. Usman, Z. H. Ren, Y. Y. Wang and Z. H. Guan, *RSC Adv.*, 2016, **6**, 107542; (*b*) Y. Y. Li, S. L. Yu, W. Y. Shen and J. X. Gao, *Acc. Chem. Res.*, 2015, **48**, 2587; (*c*) B. Jung and A. H. Hoveyda, *J. Am. Chem. Soc.*, 2012, **134**, 1490.

6 (*a*) W. Y. Li, D. F. Huang and Y. J. Lyu, *Org. Biomol. Chem.*, 2016, **14**, 10875; (*b*) K. Nogi, T. Fujihara, J. Terao and Y. Tsuji, *Chem. Commun.*, 2014, **50**, 13052; (*c*) L. Zang and Z. Hou, *Chem. Sci.*, 2013, **4**, 3395; (*d*) I. Omae, *Coord. Chem. Rev.*, 2012, **256**, 1384; (*e*) W. Wang, S. Wang, X. Ma and J. Gong, *Chem. Soc. Rev.*, 2011, **40**, 3703; (*f*) T. Fujihara, T. Xu, K. Semba, J. Terao and Y. Tsuji, *Angew. Chem., Int. Ed.*, 2011, **50**, 523.

7 Y. Tani, T. Fujihara, J. Terao and Y. Tsuji, *J. Am. Chem. Soc.*, 2014, **136**, 17706.

8 (*a*) A. D. Becke, *J. Chem. Phys.*, 1993, **98**, 5648; (*b*) C. Lee, W. Yang and G. Parr, *Phys. Rev. B: Condens. Matter Mater. Phys.*, 1988, **37**, 785; (*c*) P. J. Stephens, F. J. Devlin, C. F. Chabalowski and M. J. Frisch, *J. Phys. Chem.*, 1994, **98**, 11623.

9 (*a*) R. Yuan and Z. Y. Lin, *ACS Catal.*, 2014, **4**, 4466; (*b*) H. T. Zhao, Z. Y. Lin and T. B. Marder, *J. Am. Chem. Soc.*, 2006, **128**, 15637; (*c*) H. T. Zhao, L. Dang, T. B. Marder and Z. Y. Lin, *J. Am. Chem. Soc.*, 2008, **130**, 5586.

10 (*a*) K. Fukui, *J. Phys. Chem.*, 1970, **74**, 4161; (*b*) K. Fukui, *Acc. Chem. Res.*, 1981, **14**, 363.

11 A. V. Marenich, C. J. Cramer and D. G. Truhlar, *J. Phys. Chem. B*, 2009, **113**, 6378.

12 Y. Zhao and D. G. Truhlar, *Theor. Chem. Acc.*, 2008, **120**, 215.
13 (*a*) J. P. Foster and F. Weinhold, *J. Am. Chem. Soc.*, 1980, **102**, 7211; (*b*) A. E. Reed and F. Weinhold, *J. Chem. Phys.*, 1983, **78**, 4066.
14 M. J. Frisch, G. W. Trucks, H. B. Schlegel, G. E. Scuseria, M. A. Robb, J. R. Cheeseman, G. Scalmani, V. Barone, B. Mennucci, G. A. Petersson, H. Nakatsuji, M. Caricato, X. Li, H. P. Hratchian, A. F. Izmaylov, J. Bloino, G. Zheng, J. L. Sonnenberg, M. Hada, M. Ehara, K. Toyota, R. Fukuda, J. Hasegawa, M. Ishida, T. Nakajima, Y. Honda, O. Kitao, H. Nakai, T. Vreven, J. J. A. Montgomery, J. E. Peralta, F. Ogliaro, M. Bearpark, J. J. Heyd, E. Brothers, K. N. Kudin, V. N. Staroverov, R. Kobayashi, J. Normand, K. Raghavachari, A. Rendell, J. C. Burant, S. S. Iyengar, J. Tomasi, M. Cossi, N. Rega, J. M. Millam, M. Klene, J. E. Knox, J. B. Cross, V. Bakken, C. Adamo, J. Jaramillo, R. Gomperts, R. E. Stratmann, O. Yazyev, A. J. Austin, R. Cammi, C. Pomelli, J. W. Ochterski, R. L. Martin, K. Morokuma, V. G. Zakrzewski, G. A. Voth, P. Salvador, J. J. Dannenberg, S. Dapprich, A. D. Daniels, Ö. Farkas, J. B. Foresman, J. V. Ortiz, J. Cioslowski and D. J. Fox, *Gaussian, Inc.*, Wallingford CT, 2009.
15 (*a*) B. C. Hamann and J. F. Hartwig, *J. Am. Chem. Soc.*, 1998, **120**, 3694; (*b*) M. Kawatsura and J. F. Hartwig, *J. Am. Chem. Soc.*, 1999, **121**, 1473.
16 M. N. Birkholz, Z. Freixa and P. W. van Leeuwen, *Chem. Soc. Rev.*, 2009, **38**, 1099.
17 Q. H. Lu, B. Wang, H. Z. Yu and Y. Fu, *ACS Catal.*, 2015, **5**, 4881.